Characterization of Diesel Particles: Effects of Fuel Reformulation, Exhaust Aftertreatment, and Engine Operation on Particle Carbon Composition and Volatility

ARTICLE *in* ENVIRONMENTAL SCIENCE AND TECHNOLOGY · JUNE 2004

Impact Factor: 5.33 · DOI: 10.1021/es030129j · Source: PubMed

4 AUTHORS, INCLUDING:

Leena Rantanen
Neste Oil
18 PUBLICATIONS **276** CITATIONS

SEE PROFILE

Environ. Sci. Technol. **2004**, *38,* 2707−2714

Characterization of Diesel Particles: Effects of Fuel Reformulation, Exhaust Aftertreatment, and Engine Operation on Particle Carbon Composition and Volatility

TIMO J. A. ÅLANDER,*
ARI P. LESKINEN, AND
TAISTO M. RAUNEMAA

Laboratory for Atmospheric Physics and Chemistry, University of Kuopio, P.O. Box 1627, FIN-70211 Kuopio, Finland

LEENA RANTANEN

Engine Laboratory, Fortum Oil and Gas Oyj, P.O. Box 310, FIN-06101 Porvoo, Finland

Diesel exhaust particles are the major constituent of urban carbonaceous aerosol being linked to a large range of adverse environmental and health effects. In this work, the effects of fuel reformulation, oxidation catalyst, engine type, and engine operation parameters on diesel particle emission characteristics were investigated. Particle emissions from an indirect injection (IDI) and a direct injection (DI) engine car operating under steady-state conditions with a reformulated low-sulfur, low-aromatic fuel and a standard-grade fuel were analyzed. Organic (OC) and elemental (EC) carbon fractions of the particles were quantified by a thermal-optical transmission analysis method and particle size distributions measured with a scanning mobility particle sizer (SMPS). The particle volatility characteristics were studied with a configuration that consisted of a thermal desorption unit and an SMPS. In addition, the volatility of size-selected particles was determined with a tandem differential mobility analyzer technique. The reformulated fuel was found to produce 10−40% less particulate carbon mass compared to the standard fuel. On the basis of the carbon analysis, the organic carbon contributed 27−61% to the carbon mass of the IDI engine particle emissions, depending on the fuel and engine operation parameters. The fuel reformulation reduced the particulate organic carbon emissions by 10−55%. In the particles of the DI engine, the organic carbon contributed 14−26% to the total carbon emissions, the advanced engine technology, and the oxidation catalyst, thus reducing the OC/EC ratio of particles considerably. A relatively good consistency between the particulate organic fraction quantified with the thermal optical method and the volatile fraction measured with the thermal desorption unit and SMPS was found.

Introduction

Particles derived from diesel engines are the major constituent of urban carbonaceous aerosol, typically contributing over 70% to the total particulate elemental carbon (*1*). During recent years an increasing interest has been directed to fine atmospheric particles because epidemiological studies have proved a correlation between particle concentration and excess morbidity and mortality (*2*). Besides public health, diesel particles affect both the global climate and local air quality. Due to their catalytic properties and high specific surface area, carbonaceous particles are involved in various chemical processes in the atmosphere (*3*). The large light absorption coefficient of the carbonaceous particles results in dual effects on the atmospheric radiation balance: on one hand particles degrade solar radiation to the surface of the earth, and on the other they absorb radiation energy and hence elevate the temperature of the atmosphere. In the urban environment exhaust particles soil building materials and, due to light absoption and scattering, diminish visibility.

Diesel particles consist of a solid elemental carbon (EC) core and volatile organic carbon (OC) that is suggested to form a layer on the core. The core has typically a highly agglomerated chainlike structure, being composed of spherical primary particles ranging from 10 to 50 nm in diameter (*4*). In addition to carbonaceous species diesel particles contain water-soluble ions, among others fuel-derived sulfate, and various trace elements resulting from the use of organometallic additives in lubricant oil and abrasion of engine materials (*5*). The organic fraction has been of particular interest because it includes polycyclic aromatic hydrocarbons and their derivatives, several of which are known to be potential carcinogens and mutagens. Organic compounds in the particles are attributed to unburned, pyrolyzed or partially oxidized fuel and lubricant oil (*6*) and are transferred from the gas phase to the particulate phase by adsorption and condensation onto the existing particles or by nucleation of new particles when the exhaust cools.

The emissions of a diesel engine can be decreased by engine design and exhaust aftertreatment. An oxidation catalytic converter, which reduces carbon monoxide and gaseous hydrocarbons in diesel exhaust, also affects particulate mass emissions by reducing the organic fraction of the particles. The influence mechanism of an oxidation catalyst on the particle-bound organics is poorly understood, but direct interaction between the particles and catalyst is considered to be unlikely. Instead, the catalyst is assumed to reduce the amount of organics in the gas phase at the catalyst temperature, which results in smaller mass transfer onto the particles when the exhaust cools (*4*, *7*).

A considerable reduction of diesel emissions can be achieved also by fuel reformulation, when the net reduction is significant because it takes place over the whole vehicle fleet regardless of engine design or exhaust aftertreatment. The reduced aromatics and sulfur content in the fuel together with a higher hydrogen-to-carbon ratio influence total particulate mass emissions by reducing the organic fraction of particles. Furthermore, the lower content of aromatics in the fuel has been reported (*8*) to affect the mutagenic potential of diesel particles. For vehicles equipped with an oxidation catalyst the low fuel sulfur content has been found to be of particular importance because sulfur converts to sulfate at high catalyst operation temperatures (*7*, *9*) and, hence, may affect particulate emission rates remarkably.

In this work, the properties of particles emitted by two types of diesel engines operating with two different fuels were studied. The main objective was to characterize the effects of fuel reformulation, engine type, oxidation catalyst, and engine operation parameters on the organic and elemental carbon fractions, size, and volatile fraction of the

* Corresponding author phone: +358-17-163 237; fax: +358-17-163 229; e-mail: Timo.Olander@uku.fi.

10.1021/es030129j CCC: $27.50
Published on Web 03/16/2004

TABLE 1. Properties of Standard-Grade and Reformulated Diesel Fuels in the Tests

fuel analysis	standard	reformulated
density at 15 °C (kg/m^3)	858.1	830.6
viscosity at 40 °C (mm^2/s)	3.51	2.9
sulfur content (mg/kg)	430	27
distillation 5% by vol (°C)	223	219
distillation 95% by vol (°C)	354	348
cetane number	48.7	56.6
total aromatics (% by vol)	35.8	19.3

particles. The organic fraction of particles quantified with the thermal optical method and the volatile fraction determined with the thermal desorption are compared. Moreover, the thickness of the organic layer on the particle surface is discussed.

Experimental Section

Test Vehicles and Sampling Methods. Particle measurements were carried out with two diesel-powered passenger cars of different ages and engine types. The older one was a 1988 model Japanese-make car (odometer 250000 km), equipped with a 2.0 L naturally aspirated, indirect injection (IDI) swirl chamber engine. The newer one was a European-make 1997 turbo-charged, 1.9 L direct injection (DI) engine car (odometer 7000 km) equipped with an oxidation catalyst and an exhaust gas recirculation (EGR) system. The IDI car was employed in measurements because the new engine technology with advanced electronic control may introduce extra variables between the fuel and load parameters that cannot be controlled (*8*). To investigate the effects of the fuel, two types of summer-grade diesel fuels were applied. One was a reformulated low-sulfur, low-aromatic fuel and the other one a mixture that met the European standard EN590. The test runs with the IDI car were carried out with both fuels, whereas those with the DI car were carried out with the reformulated fuel only. The properties of the fuels are given in Table 1.

The test runs were conducted on a chassis dynamometer at the Fortum Oil and Gas Engine Laboratory. Diesel exhaust was conducted through a corrugated stainless steel tube to a dilution tunnel of 320 mm inner diameter, equipped with a constant-volume sampler (CVS) system. The dynamometer facility, the dilution tunnel, and the CVS system met the U.S. Federal Test Procedure standards. The distance from the exhaust mixing point to the sample probe was 3.4 m, which led with a dilution flow rate of 12 m^3/min to a residence time of 1.4 s. During the test runs total gas-phase hydrocarbons (THC), nitrogen oxides (NO_x), and carbon monoxide (CO) were monitored continuously. Particle measurements were carried out under steady-state operation conditions applying constant power outputs of 3.5 and 10 kW at a constant speed of 50 km/h, and of 10 and 20 kW at 80 km/h, using the fourth gear.

The applied dilution factors, relative humidities, and temperatures of diluted exhaust in the tunnel are given in Table 2. Exhaust dilution factors varied from 8:1 to 28:1 depending on the speed and engine power. Correspondingly, relative humidity varied from 30% to 42% for the IDI engine measurements and from 41% to 58% for the DI engine. Temperatures in the tunnel exceeded 52 °C in IDI engine measurements at 80 km/h, when the temperatures reached 72 °C. The ambient temperature during test runs was 23 °C.

The particle samples for gravimetric and chemical analysis were collected on 47 mm quartz fiber filters (Pallflex 2500QAR-UP), a 47 mm Teflon membrane (Gelman Zefluor P5PL047), and 142 mm Teflon-bonded glass fiber filters (Pallflex T60A20 1420). To lower the filter carbon blank level, the quartz filters

TABLE 2. Dilution Factors and Measured Temperatures and Relative Humidities in the Dilution Tunnel

fuel, speed, load	DF	*T* (°C)	RH (%)
Indirect Injection Engine			
standard fuel			
50 km/h, 3.5 kW	24.2	37.4	41.0
50 km/h, 10 kW	19.9	40.1	42.2
80 km/h, 10 kW	11.9	56.7	33.4
80 km/h, 20 kW	7.9	71.5	36.7
reformulated fuel			
50 km/h, 3.5 kW	24.5	37.1	35.8
50 km/h, 10 kW	15.5	39.0	33.2
80 km/h, 10 kW	12.1	56.1	30.2
80 km/h, 20 kW	9.5	62.5	33.6
Direct Injection Engine			
reformulated fuel			
50 km/h, 3.5 kW	27.7	33.0	41.1
50 km/h, 10 kW	18.2	35.3	47.7
80 km/h, 10 kW	14.6	42.6	51.5
80 km/h, 20 kW	9.4	52.3	57.6

were pretreated prior to sampling by heating them in a muffle furnace in air for 3 h at 900 °C. Prior to being weighed on a microbalance with a 1 μg sensitivity before and after sampling, the filters were conditioned for 24 h at a constant temperature of 20 ± 1 °C and a relative humidity of 40 ± 2%. After being weighed, the filters were closed in glass Petri dishes and stored after sampling under refrigeration at −18 °C.

Particles were sampled from the dilution tunnel isokinetically by using a probe that had a preimpactor with a cutoff size of 2 μm to withdraw coarse particles. To correct a positive sampling artifact that arises from adsorption of gaseous organic compounds on quartz fiber filter material, aerosol was sampled in two parallel lines, each having two successive filter holders (Gelman 2220). One of the lines had a quartz filter in both successive filter holders, whereas the other one had a Teflon front filter and a quartz backup. The adsorption correction was accomplished by subtracting from the quartz front filter the carbon quantified from the quartz backup behind the Teflon. The principle of this sampling method has been introduced first in ambient air sampling and is discussed in detail in refs *10* and *11*. The sampling flow rate in all measurements was 28 L/min in total, which corresponds to a filter face velocity of 20 cm/s.

Carbon and Ion Analysis. Organic and elemental carbon fractions of the particle samples deposited on quartz fiber filters were quantified by a thermal-optical transmission (TOT) method, which is based on thermal decomposition and oxidation of carbonaceous species (*12*−*15*). The carbon analyzer system applied to this study was constructed and built at the University of Kuopio. In the present system a 1 cm^2 sample punch from the quartz fiber filter is heated in a quartz tube sample oven. The oven temperature is increased first in a pure helium atmosphere in four steps to 120, 250, 450, and 550 °C, whereupon an oxidative atmosphere containing 2% oxygen and 98% helium is applied at temperatures of 550, 700, and 800 °C. Volatilized carbon from the sample punch is first oxidized in a catalyst oven to CO_2 by MnO_2 at a temperature of 915 °C, after which CO_2 is reduced to methane with hydrogen in a subsequent furnace in the presence of nickel catalyst. The carbon liberated from the sample is quantified continuously by a flame ionization detector (FID). Due to the pyrolysis process that occurs in the helium atmosphere, a portion of the organic carbon changes to elemental carbon during the analysis, resulting in sample darkening. When oxygen is added to the carrier gas, the filter becomes more transparent due to burning of

the light-absorbing elemental carbon. To correct an overestimation of the elemental carbon that results from the formation of pyrolysis products, the sample is continuously monitored by laser transmission via a 632.8 nm He−Ne laser and a photodetector. The correction is accomplished by measuring the amount of elemental carbon oxidation necessary to return the filter transmission to its value prior to the heating cycles.

To analyze sulfate, nitrate, and chloride ions, the 142 mm filters were extracted into 40 mL of deionized distilled water, where the ion concentrations were determined by ion chromatography. The ion analyses were performed in the laboratory of the Geological Survey of Finland.

Particle Size Distribution and Volatility. The size distribution of the diesel particles in the dilution tunnel was measured by a method based on particle mobility in the size range of 10−480 nm by a TSI 3934 scanning mobility particle sizer (SMPS). The SMPS consists of a TSI 3071A differential mobility analyzer (DMA) and a TSI 3022 condensation particle counter (CPC). Prior to analysis the exhaust particles were neutralized by a bipolar ^{85}Kr charger.

Particle volatility was studied with a setup that consisted of the SMPS preceded by a thermal desorption unit, where the volatile fraction of the particles was evaporated at various temperatures prior to the size spectra being measured. The desorption unit consisted of an adjustable tube furnace, 50 cm in length and 22 mm in diameter, and a subsequent annular activated charcoal unit, 50 cm in length and 12 mm in diameter, that acted as an absorber for the evaporated species, preventing them from recondensing onto the particles, when the aerosol cools.

In addition, the volatility of size-selected particles was determined with a tandem differential mobility analyzer (TDMA) technique. The TDMA method introduced by Rader and McMurry (*16*) has been applied to analysis of both evaporative and hygroscopic characteristics of combustion aerosols in several studies (*17*, *18*). In the present TDMA analysis the first DMA extracts a quasi-monodisperse size fraction from the diesel aerosol, which is subjected to the desorption unit. The change in particle size due to heat treatment is then determined with a second DMA and CPC.

Results and Discussion

Particulate Carbon Emissions. Fuel composition, exhaust aftertreatment, and engine operation all had considerable effects on the organic and elemental carbon contributions of the diesel particles. The dependence of carbon mass fractions on those parameters under steady-state driving conditions is illustrated in Figure 1. The abbreviations OC1, OC2, OC3, and OC4 denote the organic carbon fractions liberated from the sample at temperatures of 120, 250, 450, and 550 °C, and EC1, EC2, and EC3 the elemental carbon fractions liberated at temperatures of 550, 700, and 800 °C, respectively. The fraction P represents carbon formed from organic species during the analysis due to pyrolysis and is included in the organic fraction. The ion fraction represents the total mass of analyzed SO_4^{2-}, NO_3^-, and Cl^- ions.

With the IDI engine the total carbon mass emissions increased with an increase of the power output for both fuels. Changes in engine operation were observed to have a relatively small influence on the elemental carbon emission. The increase of carbon emission with increased power can thus be attributed mostly to the organic fraction, which is reflected also in the OC/EC ratios given in Figure 1.

Although the air-to-fuel ratios were not measured, it can be supposed that the increase of organic emissions may at least partially result from a reduced air-to-fuel ratio, i.e., richer combustion with a higher power output in the naturally aspirated IDI engine, which has favored the formation of incomplete combustion products. By the IDI engine the

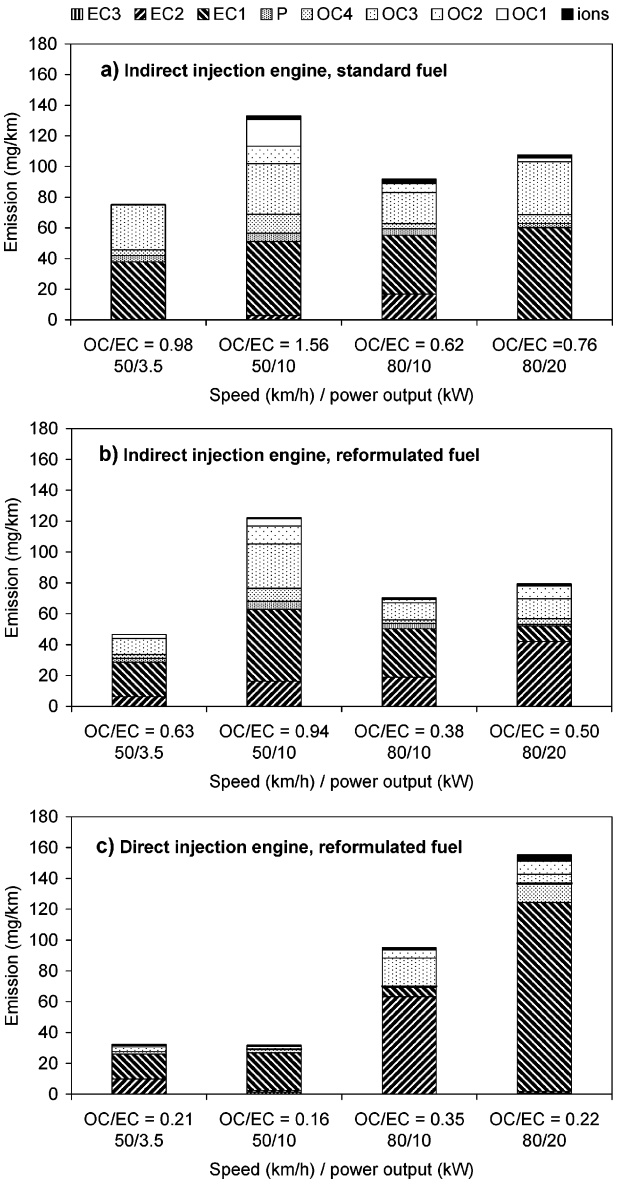

FIGURE 1. Effects of engine type, fuel composition, and engine operation on OC and EC mass emissions and the OC/EC ratio.

organic carbon in particles was composed mainly of the OC3 fraction at all speed and power values for both fuels, while the most volatile fraction OC1 was remarkable only at a speed of 50 km/h and a 10 kW power output.

The reformulated fuel resulted in 10−40% lower total carbon (TC) mass emissions compared to the standard fuel. The elemental carbon emissions remained on an average almost unchanged, and consequently, the decrease of total emissions due to fuel reformulation can be attributed predominantly to the organic fraction. The decrease in organic carbon emissions was 10−55% depending on the engine operation. This can be recognized also by OC/EC ratios, which ranged for the standard fuel from 0.62 to 1.56 as compared to the values between 0.38 and 0.94 for the reformulated fuel.

For the DI car equipped with a catalytic converter the total carbon mass emissions were at 50 km/h 30−70% lower as compared to emissions analyzed for the IDI car with the same fuel. The organic carbon emissions were reduced more than the elemental carbon (i.e., by 70−90% as compared with 10−60%). On the contrary, at 80 km/h the carbon emissions increased remarkably, being equal at 10 kW and even 50% higher at 20 kW compared to those for the IDI car

with the same fuel and engine operation. At 80 km/h the DI engine generated a large amount of elemental carbon with both power outputs. This behavior seemed to be characteristic for this engine under those operation conditions. In terms of milligrams per kilometer also the organic emissions were considerably higher at 80 km/h than at 50 km/h and closely equal to the OC emissions of the IDI car at the same speed. Instead, the OC/EC ratios were considerably lower for the DI than for the IDI car with the same fuel, which may result predominantly from the catalytic oxidation of the organics. Notable is also the behavior of OC/EC ratios of the DI car with respect to the engine operation, which in contrast to those of the IDI car decreased with increasing power. A probable reason for this may be the higher air-to-fuel ratio in the turbocharged DI engine compared to the IDI engine as well as the higher catalytic converter temperature at increased power outputs, which may have resulted in more efficient oxidation of hydrocarbons.

In consideration of the fact that only two diesel cars and fuels are involved in this investigation, the measured organic and elemental carbon emissions with respect to the engine and fuel parameters may not most obviously be representative for the real world car fleet, and therefore, a comparison with the literature is necessary. To examine the effects of fuel reformulation on diesel emissions, Durbin et al. (*19*) tested three fuels with different sulfur and aromatic contents by driving a 7.3 L turbocharged DI engine medium-duty truck in the FTP cycle. In those experiments they measured on average 18% reduction in particle mass (PM) emissions. Accordingly, Mikkonen et al. (*8*) observed that the fuel reformulation reduces the PM emissions of the light-duty DI engines by 20−40%, while the reduction for IDI engine emissions is 5−14%. The reductions of the PM emissions due to reformulation reported by both Durbin et al. and Mikkonen et al. are well comparable to the decrease of the total carbon emissions obtained in the present study. Bagley et al. (*20*) studied the effects of oxidation catalyst on the total particulate mass and soluble organic fraction (SOF) by running a naturally aspirated 7 L IDI engine in test bench. According to their observation, the catalytic aftertreatment reduced the SOF by 65% and the solid particle phase (SOL) by 35%, which resulted together in 50% reduction of total PM emissions. Under steady-state conditions at 80 km/h Kerminen et al. (*21*) measured for a 1.9 L naturally aspirated IDI engine by applying low-sulfur fuel a PM reduction of 10−30% due to catalytic oxidation. At the same time the OC/EC ratio of the particles decreased from 0.43 to 0.33, which corresponds in the case that the EC emissions have remained constant to a 25% reduction in the OC emission rate. The OC/EC ratios reported by Kerminen et al. are well comparable to the ratios measured in this study for both the IDI and DI cars with reformulated fuel at 80 km/h and 10 kW. Kleeman et al. (*22*) investigated the chemical composition of the size-fractionated diesel particles emitted by four-cylinder 3.8 L and eight-cylinder 6.5 L turbocharged medium-duty DI engine vehicles that were driven in the FTP cycle. According to their analysis, organic carbon contributed 25−40% and elemental carbon 60−70% to the total particulate depending on the size fraction. This corresponds on average to an OC/EC ratio of 0.5, which is somewhat higher than the OC/EC ratios determined for the catalyst-equipped DI car in this study. Shi et al. (*23*) investigated the effects of engine operation on particle carbon composition by running a four-cylinder 4 L turbocharged DI engine in test bench at 25%, 50%, and 100% loads with two constant engine speeds. They determined the organic carbon to contribute 24−78% and the elemental carbon 25−52% to the total PM. This corresponds to OC/EC ratios of 0.47−2.3, thus indicating considerably higher OC contributions than measured in the present study. According to Shi et al. (*23*), the OC/EC ratio

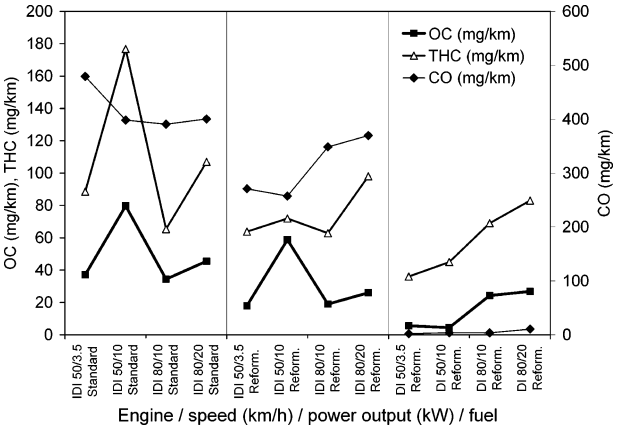

FIGURE 2. Dependence of particulate organic carbon, carbon monoxide, and total hydrocarbon emissions on the engine type, fuel, and engine operation.

decreased with increasing power output, an observation which is consistent with the behavior of the DI engine particles analyzed in this study.

In Figure 2 are plotted the particulate OC emissions together with total gaseous hydrocarbon and carbon monoxide emissions with respect to engine operation and fuel and engine type. The particulate organic emissions depend on those parameters consistently with the THC emissions. The very similar behavior of the particulate and gaseous organic emissions suggests a close interaction between the gas and particulate phases and consequently points out that the organic fraction in particles is predominantly not formed from the gas-phase organics until the exhaust cools in the tailpipe and exhaust plume. On the contrary, the CO emissions behaved differently with the IDI car with respect to power output. With the DI car the CO emissions were reduced drastically compared to particulate OC and THC emissions, showing that the oxidation catalyst converts CO more efficiently than hydrocarbons.

Particle Size and Particle Emission Rate. In a dilution tunnel at a certain range of dilution ratios a supersaturation of volatile species (i.e., sulfate and hydrocarbons) can occur, which may result in formation of new nuclei mode particles (*24*). However, in this investigation the measured size distributions were unimodal for both fuels and engines at all operation modes (i.e., the nucleation mode did not appear under any applied dilution condition). The effects of engine and fuel parameters on particle number emission rates in the size range of 10−480 nm is depicted in Figure 3. The emission rates with respect to engine operation are consistent with the carbon mass emissions shown in Figure 1 except for the IDI engine with the reformulated fuel at a speed of 80 km/h with a 10 kW output. The particle number emission rates at 80 km/h were considerably higher than could be expected on the basis of the mass emissions.

The influence of engine operation on the exhaust particle size with the fuel and engine type as a parameter is shown also in Figure 3. Particles emitted by the IDI car had a count median diameter (CMD) ranging from 63 to 77 nm, while the particle size appeared to be only slightly affected by the engine operation. The particles produced with reformulated fuel had a CMD on an average 2 nm smaller compared to particles produced with the standard fuel. Instead, the engine type affected the particle size considerably, as the particles produced by the DI engine had a CMD 30−40 nm larger than the particles emitted by the IDI engine. The operation parameters of the DI engine influenced the particle size remarkably, when the increase of the power output from 10 kW at 50 km/h to 20 kW at 80 km/h increased the CMD by about 15 nm.

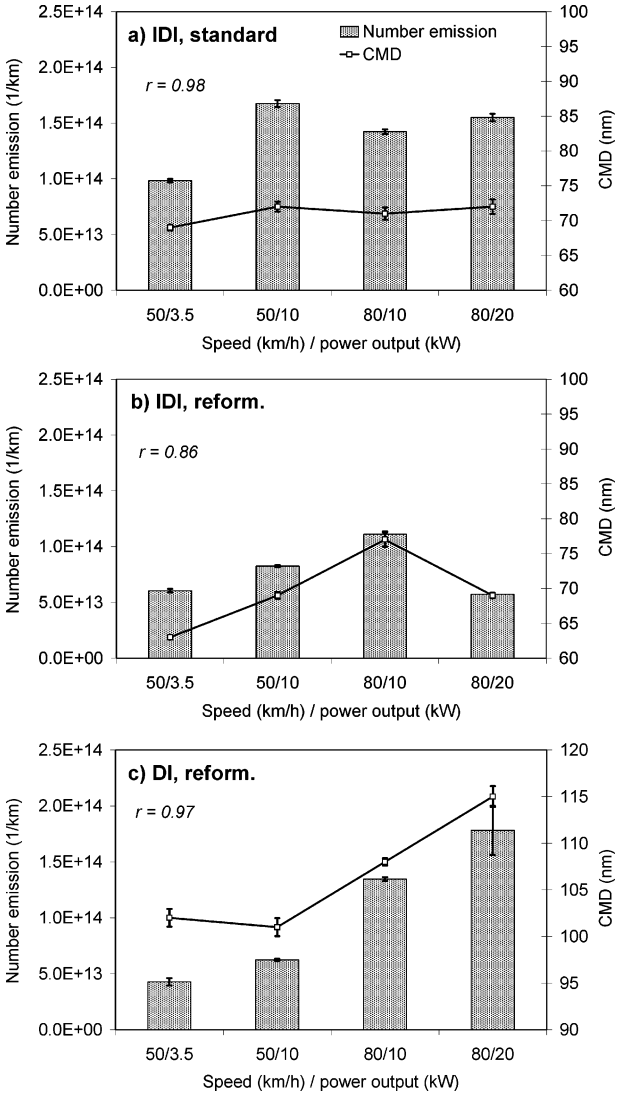

FIGURE 3. Effects of engine type, fuel composition, and engine operation on particle number emission rates and particle CMDs. Note the different CMD scale in panel c. *r* stands for the correlation coefficient between the number emission and CMD.

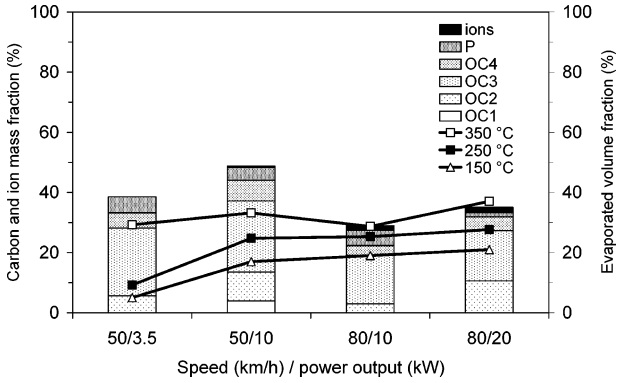

FIGURE 4. Comparison between the organic carbon mass and volatile volume fractions of the particles emitted by the IDI engine with the reformulated fuel. Bars denote the organic carbon and ion mass fractions analyzed with the thermal-optical method and an ion chromatograph, and lines denote the volume fraction determined with the desorption unit and SMPS analysis at three evaporation temperatures. The volatile volume fractions are corrected for diffusion and thermophoretic losses. Symbols are as follows: ions = SO_4^{2-}, NO_3^-, and Cl^-; P = pyrolysis correction; OC1, OC2, OC3, OC4 = organic fraction.

When comparing the effects of engine operation on CMD, one can find that CMD correlates well with the number emission rates with a correlation coefficient of 0.86−0.98. The particle number concentration in the dilution tunnel and exhaust transfer line increased with the particle emission rate, the good correlation suggesting that the CMD has been affected at least partially by a coagulation process in the tunnel.

The measured CMDs regarding the IDI car are quite a similar to the diesel exhaust particle sizes presented in the literature (*20*). On the contrary, the exhaust particle CMDs measured for the DI engine in this study seem to be exceptionally large as compared to geometric means of 50−70 nm measured by Shi et al. (*23*) and Maricq et al. (*25*). As the dilution and measuring conditions were equal for both engines, the larger size of the particles emitted by the DI car is predominantly attributable to the engine itself, even though the above-mentioned coagulation has most obviously increased the particle size emitted at 80 km/h. However, in the absence of a parallel experiment with a similar car it is unclear whether the large particles were characteristic for the engine type or for this individual engine only.

Thermal Desorption Analysis. The volatile fraction of diesel exhaust particles consists of organic carbon, water-soluble ions such as sulfate, sulfuric acid, and water. The dependence of volatile volume fractions on the engine operation analyzed with the desorption unit and SMPS at three evaporation temperatures is illustrated in Figure 4.

The particle losses in the desorption unit were predicted theoretically to correct the evaporation experiments for losses. The sedimentation losses are negligible for submicrometer particles (*26*, *27*), and hence, only diffusion and thermophoresis were considered. The losses of the desorption unit as well as evaporation efficiency are discussed in more detail elsewhere (*27*, *28*).

The diffusion loss through the tube in terms of penetration, P_{diff}, is obtained (*26*, *27*) from the equation

$$P_{diff} = 1 - 2.56\zeta^{2/3} + 1.2\zeta + 0.177\zeta^{3/4} \quad \zeta \le 0.02 \quad (1)$$

where ζ is the dimensionless deposition parameter:

$$\zeta = \frac{DL}{r^2 U} \quad (2)$$

In eq 2, L is the tube length, r is the tube radius, and U is the aerosol flow velocity. The diffusion coefficient D for particle deposition is given (*27*, *28*) by the equation

$$D = \frac{kTC_c}{3\pi\mu d} \quad (3)$$

where k is the Boltzmann constant, T is the absolute temperature, C_c is the Cunningham slip correction factor, μ is the dynamic viscosity, and d is the particle diameter.

The penetration due to thermophoretic losses, P_t, is calculated (*27*, *29*) from the equation

$$P_t = 1 - \frac{(Pr)K\phi_0}{\theta^*} \quad (4)$$

where Pr is the dimensionless Prandtl number

$$\phi_0 = \frac{\theta^*}{1 + \theta^*} \quad (5)$$

and

$$\theta^* = \frac{T_{min}}{T_{max} - T_{min}} \quad (6)$$

where T_{min} and T_{max} are the temperatures of the tube wall and entering gas, respectively. The thermophoretic coefficient K is obtained from the equation

$$K = 2C_s \frac{\frac{k_g}{k_p} + C_t\frac{\lambda}{a}\left[1 + \frac{\lambda}{a}(1.2 + 0.41e^{-0.88a/\lambda})\right]}{\left(1 + 3C_m\frac{a}{\lambda}\right)\left(1 + 2\frac{k_g}{k_p} + 2C_t\frac{\lambda}{a}\right)} \quad (7)$$

where k_g and k_p are the thermal conductivities of air and carbon particles and λ is the gas mean free path, a the particle radius, $C_s = 1.17$ the thermal slip coefficient, $C_m = 1.14$ the momentum exchange coefficient, and $C_t = 2.18$ the temperature jump coefficient (*27*, *30*).

To determine the temperatures T_{min} and T_{max}, the axial temperature profiles in the centerline and tube wall of the desorption unit were measured at evaporation temperatures of 150, 250, and 350 °C. On the basis of these measurements, penetrations of 75−94% were calculated in the size range of 10−480 nm at the 350 °C desorption temperature.

Particles for the evaporation analysis illustrated in Figure 4 were produced by the IDI engine with the reformulated fuel. The evaporation volume fractions were calculated in the size range of 10−480 nm from the volume distributions at the corresponding desorption unit temperatures by assuming spherical particles. The highest desorption temperature 350 °C was assumed to be sufficiently high to evaporate volatile hydrocarbons, but low enough to not oxidize elemental carbon (*12*, *26*). The organic carbon and ion mass fractions analyzed with the thermal optical method and ion chromatograph are given as stacked bars in the same figure for comparison.

The volatile volume fractions of the particles emitted at 80 km/h accounted for 30−38% of the total particle volume at the 350 °C evaporation temperature, which agreed well with the analyzed total OC and ion mass fractions. Instead, at 50 km/h the volatile fractions contributed only 30−35% to the total volume, which were 10−15% units lower than the analyzed OC and ion mass fractions. At the 150 and 250 °C desorption temperatures the evaporated fractions were considerably lower, ranging from 15% to 25% at every engine operation mode except for at the 3.5 kW power output, where the evaporated volume was below 10%.

Besides the density of organic matter that differs from unity, several factors in the thermal desorption analysis give rise to the differences observed between the evaporation volume and the organic carbon mass fractions. The determination of the volatile fraction with a thermodesorber and size analysis is based on the changes in the mobility equivalent diameter, which includes uncertainties due to the actual, very irregular shape of diesel agglomerates. Nonetheless, the calculations in this study are based on a simple assumption of spherical particles, because the fractal models require detailed information about the particle morphology or include assumptions regarding the fractal structure, which may also introduce uncertainties in particle volume calculations.

Because the volatile matter does not necessarily cover the particles uniformly but may collect in pores and intraparticle cavities between the primary particles (*31*), even a considerable decrease in the particle volume due to evaporation does not result in a significant change in the mobility diameter. This leads to underestimation of the volatile fraction and can be the reason for the low evaporated

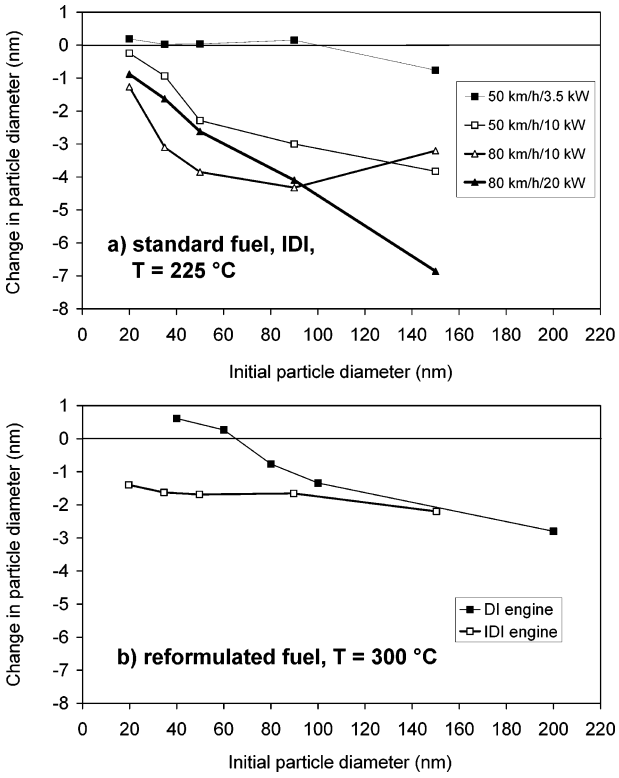

FIGURE 5. Changes in mobility diameters of size-selected diesel particles due to heat treatment as measured with a TDMA method: (a) standard fuel, (b) reformulated fuel.

volume fractions measured for the particles emitted at 50 km/h. On the other hand, the collapse of the agglomerate structure at elevated temperature is also possible, when the decrease in the mobility diameter is attributed predominantly to a denser package of the particles, resulting in overestimation of the volatile fraction. Moreover, by assuming a log-normal size distribution with a CMD of 70 nm and a standard deviation of 1.77, one can calculate that the analyzed size range between 10 and 480 nm represents approximately only 90% of the particle volume subjected to carbon analysis, which may introduce small uncertainties, as the OC/EC ratio may not be constant over the particle size range. Despite the uncertainties in the interpretation of the analysis results, the volatile volume fractions of particles quantified at 350 °C agreed fairly well with the OC fractions by overestimating them at a maximum by 2 and underestimating by 15% units. Thus, the desorption unit with particle size analysis seems to provide an applicable method for analysis of the organic fraction of combustion aerosol particles.

The volatility analysis of size-selected diesel particles was performed at five particle diameter values in the range of 20−150 nm with the IDI engine and in the range of 40−200 nm with the DI engine. The analyzed size range was limited on the both ends due to a low number of particles, and hence, the analysis represents approximately only one-third of the particle volume subjected to carbon analysis, and about half the volume of the 10−480 nm sized particles subjected to the thermal desorber and size analysis. Figure 5a illustrates the analysis of the particles emitted by the IDI engine with the standard fuel at four engine operation modes by applying the 225 °C desorption unit temperature. Correspondingly, the analysis of the particles produced by the IDI and DI engines with the reformulated fuel at 50 km/h and a 3.5 kW power output at the desorption unit temperature of 300 °C is shown in Figure 5b.

The changes in the mobility diameter of 20 and 40 nm particles due to heat treatment were measured to be a

maximum of about 1 nm for both fuels and engines at all operation parameters. This suggests that particles are solid consisting of single or small clusters of soot primary particles covered by a thin layer of volatile matter. At the 225 °C evaporation temperature the size of the particles emitted by the IDI car with a 3.5 kW power output remained in practice unaffected in the 20−90 nm size range, while at the 300 °C desorption temperature the size of the 40−60 nm particles emitted by the DI car at the corresponding engine operation mode even slightly increased. Because the particle growth due to heat treatment is not probable, the result is most obviously attributed to the deviation of measurement. The observed particle growth lies within an accuracy of ±0.5 nm that can be proposed for the TDMA method in this particle size range. Instead, the shrinkage of the larger particles was found to increase with particle size with both fuels and engines as well as operation parameters. The largest quantified size decrease was 7 nm for a particle of 150 nm size, but it can be proposed that stronger shrinkage might be possible by larger particles outside of the analysis range. The measured change in particle diameter suggests that the thickness of the volatile coverage is not uniform over the size range, but increases with particle diameter. However, the interpretation for particle shrinkage is not unambiguous due to the complexity of the agglomerate structure that rises with increasing particle size. The increased shrinkage in the mobility diameter due to heat treatment may be at least partially attributed to the collapse of the agglomerates (*32*). On the other hand, in carbon analyses of the size-resolved submicrometer diesel particles, the OC/EC ratio has been quantified to be roughly constant (*22*) or even increase (*21*) with particle diameter. Thus, because the organic volume is proportional to the third power of the particle diameter, the coverage thickness on the surface must increase with increased particle size.

Kwon et al. (*33*) have analyzed the volatility of size-selected diesel nanoparticles with almost similar TDMA setups. The particles were produced for analysis with a 3.4 L DI engine truck operating at idling and half-load conditions. The initial sizes of the monodisperse aerosol particles extracted by the first DMA and subjected to thermal desorption were in the half-load experiment 32.5, 50, and 75.5 nm. In their experiment, above the evaporation temperature of 200 °C the monodisperse aerosol dispersed into two modes, the smaller mode consisting of semivolatile matter and the larger one of solid particles. At a temperature of 300 °C the geometric mean diameter of the semivolatile mode has shrunk 13.5−22 nm compared to the initial size, showing that the particles, in contrast to this study, contained a high amount of volatile material. On the contrary, the shrinkage of the solid mode was only 0.5−2.5 nm, which agrees with the particle shrinkage determined in this study.

The average thickness of the organic coverage layer can be roughly estimated on the basis of the OC/EC ratio if the specific surface area and the density of the organic layer are known (*34*). By assuming spherical carbon particles having a density of 1 g/cm^3, the specific surface area of 37−42 m^2/g for the IDI engine with the standard fuel and the area of 41−45 m^2/g for the particles produced with the reformulated fuel can be calculated from the measured size distributions. Similarly, the specific area of 29−33 m^2/g for the DI engine is obtained. By converting the organic mass fractions given in Figure 1 to volume by applying the unit density and dividing the organic volume by the surface area, the estimates of 10−14 nm and, respectively, 6−11 nm are calculated for the organic coverage thickness of the particles emitted by the IDI car with the standard and the reformulated fuels. The layer thickness of 5−8 nm similarly follows for the particles emitted by the DI car. These estimates, however, are considerably higher than can be expected on the basis of the particle shrinkage quantified in thermal analysis, and it is obvious that the assumption of spherical particles underestimates the area of carbon agglomerates. By applying a specific surface area of 100 m^2/g that McDow et al. (*31*) considered to be a reasonable upper limit for the elemental carbon surface, average layer thicknesses of 4−6 nm for the standard fuel and 3−5 nm for the reformulated fuel with the IDI engine and 1−3 nm for the DI engine would result. These values, in consideration of the fact that they are based on the assumption of uniform coverage over the particle size range, agree well with the observed particle shrinkage.

Acknowledgments

This work was carried out under the MOBILE Program funded by the National Technology Agency of Finland (Tekes). The financial support by the Academy of Finland is also gratefully acknowledged. We acknowledge the technical assistance of Mr. Ismo Ruotsalainen and Mr. Lasse Laitinen from the University of Kuopio in aerosol sampling and the technical assistance of Mr. Pertti Gustafsson and Mr. Jari Sorvari from the Fortum Oil and Gas Oy Engine Laboratory in the test runs.

Literature Cited

(1) Hamilton, R. S.; Mansfield, T. A. *Atmos. Environ.* **1991**, *25*, 715−723.
(2) Pope, C. A., III; Thun, M. J.; Namboodiri, M. M.; Dockery, D. W.; Evans, J. S.; Speizer, F. E.; Heath, C. W. *Am. J. Respir. Crit. Care Med.* **1995**, *151*, 669−674.
(3) Chang, S. G.; Brodinsky, R.; Gundel, L. A.; Novakov, T. In *Particulate Carbon: Atmospheric Life Cycle*; Wolf, G. T.; Klimish, R. L., Eds.; Plenum: New York, 1982; pp 159−181.
(4) Johnson, J. H.; Bagley, S. T.; Gratz, L. D.; Leddy, D. G. *SAE Tech. Pap. Ser.* **1994**, *No. 940233*.
(5) Abdul-Khalek, I. S.; Kittelson, D. B.; Graskow, B. R.; Wei, Q.; Brear, F. *SAE Tech. Pap. Ser.* **1998**, *No. 980525*.
(6) Rogge, W. F.; Hildemann, L. M.; Mazurek, M. A.; Cass, G. R.; Simoneit, B. R. T. *Environ. Sci. Technol.* **1993**, *27*, 636−651.
(7) Klein, H.; Lox, E.; Kreuzer, T.; Kawanami, M.; Ried, T.; Bächmann, K. *SAE Tech. Pap. Ser.* **1998**, *No. 980196*.
(8) Mikkonen, S.; Kiiski, U.; Mäkelä, M.; Niemi, A.; Niemi, M.; Rantanen, L.; Saikkonen, P. *SAE Tech. Pap. Ser.* **1997**, *No. 971634*.
(9) Lange, W. W.; Schäfer, A.; Le'Jeune, A.; Naber, D.; Reglizky, A. A.; Gairing, M. *SAE Tech. Pap. Ser.* **1993**, *No. 932685*.
(10) McDow, S. R.; Huntzicker, J. J. *Atmos. Environ.* **1990**, *24*, 2563−2571.
(11) Turpin, B. J.; Huntzicker, J. J.; Hering, S. V. *Atmos. Environ.* **1994**, *28*, 3061−3071.
(12) Huntzicker, J. J.; Johnson, R. L.; Shah, J. J.; Cary R. A. In *Particulate Carbon: Atmospheric Life Cycle*; Wolf, G. T., Klimish, R. L., Eds.; Plenum: New York, 1982; pp 79−88.
(13) Johnson, R. L., Shah, J. J., Cary, R. A., Huntzicker, J. J. In *Atmospheric aerosol source/Air quality relationships*; Macias, E. S., Hopke, P. K., Eds.; ACS Symposium Series 167; American Chemical Society: Washington, DC, 1981; pp 223−233.
(14) Chow, J. C.; Watson, J. G.; Pritchett, L. C.; Pierson, W. R.; Frazier, A. C.; Purcel, R. G. *Atmos. Environ.* **1993**, *27*, 1185−1201.
(15) Watson, J. G.; Chow, J. C.; Lowenthal, D. H.; Pritchett, L. C.; Frazier, C. A.; Neuroth, G. R.; Robbins, R. *Atmos. Environ.* **1994**, *28*, 2493−2505.
(16) Rader, D. J.; McMurry, P. H. *J. Aerosol Sci.* **1986**, *17*, 771−787.
(17) Kauffeldt, Th.; Schmidt-Ott, A. *J. Aerosol Sci.* **1998**, *29*, S625 − S626.
(18) Weingartner, E.; Burtscher, H.; Baltensperger, U. *Atmos. Environ.* **1997**, *31*, 2311−2327.
(19) Durbin, T. D.; Zhu, X.; Norbeck, J. M. *Atmos. Environ.* **2003**, 2105−2116.
(20) Bagley, S. T.; Gratz, L. D.; Johnson, J. H.; McDonald, J. F. *Environ. Sci. Technol.* **1998**, *32*, 1183−1191.
(21) Kerminen, V. M.; Mäkelä, T. E.; Ojanen, Ch. H.; Vilhunen, J. K.; Rantanen, L.; Havers, N.; von Bohlen, A.; Klockow, D. *Environ. Sci. Technol.* **1997**, *31*, 1883−1889.
(22) Kleeman, M. J.; Schauer, J. J.; Cass, G. R. *Environ. Sci. Technol.* **2000**, *34*, 1132−1142.
(23) Shi, J. P.; Mark, D.; Harrison, R. M. *Environ. Sci. Technol.* **2000**, *34*, 748−755.

(24) Kittelson, D. B. *J. Aerosol Sci.* **1998**, *29*, 575−588.
(25) Maricq, M. M.; Chase, R. E.; Xu, N.; Laing, P. M. *Environ. Sci. Technol.* **2002**, *36*, 283−289.
(26) Burtscher, H.; Baltensperger, U.; Bukowiecki, N.; Cohn, P.; Hüglin, C.; Mohr, M.; Matter, U.; Nyeki, S.; Schmatloch, V.; Streit, N.; Weingartner, E. *J. Aerosol Sci.* **2001**, *32*, 427−442.
(27) Abdul-Khalek, I. S.; Kittelson, D. B. *SAE Tech. Pap. Ser.* **1995**, *No. 950236*.
(28) Brockman, J. E. In *Aerosol Measurement: Principles, Techniques, and Applications*; Willeke, K., Baron, P. A., Eds.; Van Nostrand Reinhold: New York, 1993; Chapter 6.
(29) Walker, K. L.; Homsy, G. M.; Geyling, F. T. *J. Colloid Interface Sci.* **1978**, *69*, 133.
(30) Talbot, L.; Cheng, R. K.; Schefer, R. W.; Willis, D. R. *J. Fluid Mech.* **1980**, *101*, 737−758.
(31) McDow, S. R.; Jang, M.; Hong, Y.; Kamens, R. M. *J. Geophys. Res.* **1996**, *101*, 19 593−19 600.
(32) Schmidt-Ott, A. *J. Aerosol Sci.* **1988**, *19*, 553−563.
(33) Kwon, S. B.; Lee, K. W.; Saito, K.; Shinozaki, O.; Seito, T. *Environ. Sci. Technol.* **2003**, *37*, 1794−1802.
(34) Ross, M. M.; Risby, T. H.; Steele, W. A.; Yasbin, R. E. *Colloids Surf.* **1982**, *5*, 17−31.

Received for review September 22, 2003. Revised manuscript received February 2, 2004. Accepted February 11, 2004.

ES030129J